Journal of Natural Gas Science and Engineering 26 (2015) 1200–1212

Contents lists available at ScienceDirect

Journal of Natural Gas Science and Engineering

journal homepage: www.elsevier.com/locate/jngse

Mineralogical, microstructural and physiochemical characteristics of organic-rich shales in the Sichuan Basin, China

Lixi Liang, Jian Xiong, Xiangjun Liu*

State Key Laboratory of Oil and Gas Reservoir Geology and Exploitation, Southwest Petroleum University, Chengdu, 610500, China

ARTICLE INFO

Article history:
Received 28 May 2015
Received in revised form
9 August 2015
Accepted 10 August 2015
Available online 14 August 2015

Keywords:
Sichuan Basin
Upper Longmaxi Formation
Lower Longmaxi Formation
Mineralogical characteristics
Microstructural characteristics
Physiochemical characteristics

ABSTRACT

Although the Lower Silurian Longmaxi Formation shales in the Sichuan Basin have been widely investigated for their shale gas potential, detailed research on the differences between the Upper Longmaxi Formation (ULF) shales and the Lower Longmaxi Formation (LLF) shales is still scarce. In this study, the divergent properties of the LLF and ULF shales in the Sichuan Basin of China were investigated, including mineralogical characteristics, microstructural characteristics and physiochemical characteristics. The mineralogical characteristics and their influences, the relationships between the specific surface area, pore volume and TOC, mineralogical compositions, and the influences of microstructure on the development of the Longmaxi Formation (LF) shale gas reservoir were explored and discussed. The results indicate that the LF shales mainly consist of quartz and clay minerals. The ULF shales have higher clay minerals contents and lower quartz contents, whereas the LLF shales have lower clay minerals contents and higher quartz contents. Compared with the ULF shales, the LLF shales have higher TOC contents, which results in higher specific surface area and total pore volume, a larger fractal dimension, a more complex pore structure and thus a greater adsorption capacity. The LLF shales have weaker hydration swelling and stronger brittle features, indicating that the LLF shales would have good wellbore stability and good hydraulic fracturing. Because of fractures in the LF shale formation, designs for oil-based or water-based drilling fluid systems need to consider sealing technologies. For water-based drilling systems, hydration inhibition should be considered, especially for the ULF shale formation.

1. Introduction

With increasing demand for energy and advances in exploration and development technologies, the exploitation of unconventional oil and gas reservoirs, especially shale gas reservoirs, has attracted the attention of many countries. In 2013, a study conducted by the U.S. DOE's Energy Information Administration estimated shale gas resources at 36.1 $\times$ 10^{12} m^3 in China and 17.75 $\times$ 10^{12} m^3 in the Sichuan Basin (EIA, 2013). Another study, issued by the Ministry of Land and Resources of the People's Republic of China, estimated the shale gas resources to be approximately 25.08 $\times$ 10^{12} m^3 in China and 4.42 $\times$ 10^{12} m^3 in the Sichuan Basin (MRL, 2012). These studies suggest significant development potential for shale gas resources in the Sichuan Basin of China. There are several shale strata in the Sichuan Basin, including the Upper Triassic Xujiahe Formation, the Lower Silurian Longmaxi Formation, the Upper Ordovician Wufeng Formation and the Lower Cambrian Niutitang Formation (Qiongzhusi Formation). The first commercial exploitation of a shale gas reservoir in China occurred in the Jiaoshiba region of the southeastern Sichuan Basin, and the Changning-Weiyuan national demonstration area has been established in the Changning region in the southern Sichuan Basin. Both projects aim to exploit Lower Silurian Longmaxi Formation shales. Zeng et al. (2011) and Huang et al. (2012) noted that the Lower Silurian Longmaxi Formation has high development potential, indicating its potential as a shale gas reservoir.

At present, a large number of studies have investigated the Longmaxi Formation shales in the Sichuan Basin, including examinations of its accumulation conditions and mechanisms (Huang et al., 2011; Liang et al., 2012; Liu et al., 2013; Zhang et al., 2013; Wang et al., 2014), mineralogical characteristics (Chen et al., 2011a, 2011b; Wang et al., 2012; Chen et al., 2013a; Guo and Zhang, 2014), geochemical characteristics (Wang et al., 2009; Zeng et al., 2011; Chen et al., 2013b; Dai et al., 2014), pore structural characteristics (Chen et al., 2012, 2013a; Bai et al., 2013; Tian et al., 2013; Hou et al., 2014; Tang et al., 2015), adsorption

* Corresponding author.
E-mail addresses: liuxiangjunswpi@163.com, 13880093092@163.com (X. Liu).

http://dx.doi.org/10.1016/j.jngse.2015.08.026
1875-5100/

characteristics (Wu et al., 2012; Guo et al., 2013; Xue et al., 2013; Hou et al., 2014; Zhou et al., 2014) and mechanical characteristics (Liang et al., 2014; Cheng et al., 2015; Heng et al., 2015; Liang et al., 2015). Based on the lithology of the Lower Silurian Longmaxi Formation, Chen et al. (2011a) and Bai et al. (2013) suggest that it should be divided into a Lower Longmaxi Formation (LLF) and an Upper Longmaxi Formation (ULF), as exemplified by the Longmaxi Formation stratigraphic section of Shuanghe in the Changning area of the Sichuan Basin. The dichotomous characteristics of the Longmaxi Formation (LF) shales include differences in mineralogical, geochemical, microstructural and physiochemical characteristics between the segments. However, few studies have investigated these differences in detail.

The mission of this paper is to investigate the different properties of the LLF shales and the ULF shales in the Sichuan Basin of China, including mineralogical characteristics, microstructural characteristics and physiochemical characteristics. We examine core samples from the Jiaoshiba shale gas field in the southeast Sichuan Basin and outcrop samples from the Changning district in the southern Sichuan Basin by applying X-ray diffraction (XRD) analysis, total organic carbon (TOC) analysis, cation exchange capacity (CEC) analysis, contact angle measurements, low-pressure N_2 adsorption analysis and scanning electron microscope (SEM) observations. We describe the mineralogical characteristics and their influences, the relationships between specific surface area, pore volume, and TOC, mineralogical compositions, and the influences of microstructure on the development of the Longmaxi Formation shale gas reservoir. We anticipate that our results will facilitate the exploration of the LF shale gas reservoirs in the Sichuan Basin.

2. Samples and methods

2.1. Samples

Shale samples were obtained from the Lower Silurian Longmaxi Formation in the Sichuan Basin of China, including outcrop samples and core samples. The outcrop samples were collected from the Changning district in the southern Sichuan Basin (Area 1), and the core samples were collected from the JY 4 shale gas well in the Jiaoshiba shale gas field in the southeastern Sichuan Basin (Area 2). These samples demonstrate the dichotomy in the lithological profile of the LF shales, which are divided into the ULF shales and the LLF shales. The lithology of the ULF shales that were deposited in a shallow continental shelf environment consists of grey silty shale, mudstone shale and siltstone shale, whereas the LLF shales that were deposited in a deep continental shelf environment are black shales. The ULF shales are located at N28 °23′38.5″, E104°52′55.5″ and N28 °23′15.3″, E104°52′55.0″ and the LLF shales are located at N28 °23′52.6″, E104°52′24.2″. Sampling, breaking and sieving were conducted according to national standards, after which the samples were analysed in an experimental program including XRD analysis, TOC analysis, CEC analysis, contact angle measurements, low-pressure N_2 adsorption analysis and scanning electron microscope (SEM) observations. Based on the results of the low-pressure N_2 adsorption analysis, the fractal dimensions of the LF shales were calculated with the fractal FHH equation.

In this study, XRD analysis was conducted on 30 outcrop samples from the Changning area and 48 core samples from the JY 4 well, TOC analysis was conducted on 16 outcrop samples from the Changning area and 48 core samples from the JY 4 well, CEC analysis was conducted on 30 outcrop samples from the Changning area and 9 core samples from the JY 4 well, contact angle measurements were taken on 20 outcrop samples from the Changning area, and low-pressure N_2 adsorption analysis was conducted on 16 outcrop samples from the Changning area. In addition, researchers also collected 6 outcrop samples from the Changning area for SEM observations.

2.2. Experimental methods

The shale samples were crushed to 100 mesh size grains for XRD analysis with an X'Pert PRO. The mineralogical composition and relative mineral percentage of the samples were estimated following the Chinese Oil and Gas Industry Standards SY/T5983-1994 and SY/T5163-1995.

Shale samples were crushed to 100 mesh size grains and treated with hydrochloric acid to remove carbonates before TOC analysis on a LECO CS230 carbon/sulphur analyser according to Chinese National Standards GB/T19145-2003 and GB/T18602-2001.

The shale samples were crushed to 100 mesh size grains for CEC analysis. The methylene blue test shown in Eq. (1) was used to calculate the CEC of the LF shales. The experimental process followed the Chinese Oil and Gas Industry Standards SY/T 5613-2000 and SY/T 5613-93.

$$\mathrm{CEC} = a/b \times 100 \tag{1}$$

In the above equation, CEC is the cation exchange capacity of the shales; a is one millilitre of methylene blue solution; and b is the mass in grams of the shale during the titration process.

The shale samples were crushed to 60–80 mesh size grains and then outgassed at 378 K for 24 h for low-pressure N_2 adsorption analysis using a Quadrasorb™ SI Surface Area Analyser and Pore Size Analyser following Chinese National Standards GB/T19587-2004 and GB/T 21650.2-2008. The N_2 adsorption isotherms of all of the shale samples were measured for relative pressures varying from 0.01 to 0.995 at 77 K. The N_2 adsorption/desorption isotherms provide information on the specific surface area and total pore volume. The specific surface area was calculated with the multi-point BET (Brunauer–Emmett–Teller) method, using the N_2 adsorption data under the relative pressure range of 0.05–0.30 (Brunauer et al., 1938).

Fractal theory can be used to describe the pore structural properties of a solid (Pfeifer and Avnir, 1983; Avnir and Jaroniec, 1989), and fractal dimension, an index of the surface roughness or structural irregularity of a solid, can be used for quantitative evaluation of fractal geometry (Pfeifer and Avnir, 1983). Based on the N_2 adsorption data, the fractal dimension was calculated with the fractal FHH equation, presented as follows (Yao et al., 2008):

$$\ln(V) = (\mathrm{D} - 3)\ln(\ln(p_o/p)) + \text{constant} \tag{2}$$

where V is the volume of N_2 adsorbed at each equilibrium pressure p; p_o is the saturation pressure of N_2. From Eq. (2), we observe that the relationship between $\ln(V)$ and $\ln(\ln(p_0/p))$ is linear and that the slope of the plot of $\ln(V)$ versus $\ln(\ln(p_0/p))$ can be used to calculate the fractal dimension according to Eq. (2).

We performed wettability experiments to investigate the wetting behaviour of LF shale samples. The low permeability and porosity of LF shale makes it difficult to use the Amott and USBM methods to investigate its wettability. Therefore, contact angle measurements were used to quantitatively evaluate wettability. The gas–liquid-rock contact angles were measured using a DSA100 optical contact angle-measuring instrument.

To observe the mode of occurrence, the arrangement of the clay minerals and the microstructure characteristics of the LF shales, we utilized a Quanta450 scanning electron microscope in high vacuum scanning mode. Using different working voltages, the Quanta 450 can reach a resolution ratio of 3 nm and has a magnification power of 25–200000×. To prepare the samples, we etched their surfaces

with argon ion polishing to create a mirror surface, which avoids the damage caused by normal polishing techniques and maintains the true pore morphology. Finally, we applied a gold film to the sample surface.

3. Results

3.1. Mineralogical compositions

The XRD analysis results of the LF shale samples from Area 1 and Area 2 are shown in Figs. 1 and 2, respectively. These results show that the LF shales in Areas 1 and 2 are mainly composed of quartz, feldspar (orthoclase and plagioclase), potash feldspar and plagioclase, carbonates (calcite and dolomite), clay minerals (illite, illite/smectite and chlorite) and a small amount of pyrite. In Fig. 1, we observe that the clay minerals contents of the Area 1 LF shale samples ranges from 11.1% to 63.6%, with an average of 33.3%; the quartz contents range from 20.08% to 62.66%, with an average of 38.70%; and the carbonates contents range from 8.76% to 39.59%, with a mean value of 22.10%. The clay minerals are primarily illite and do not contain swelling minerals, such as montmorillonite; the average illite content is over 70%. In Fig. 2, we note that the clay minerals contents of the LF shale samples in Area 2 ranges from 21.45% to 65.94%, with an average of 38.27%; the quartz contents range from 25.12% to 51.04%, with an average of 37.39%; and the carbonates contents range from 0.38% to 19.04%, with a mean value of 10.61%. The clay minerals are primarily illite with no swelling minerals, such as montmorillonite, and the average illite content is over 70%. Figs. 1 and 2 demonstrate differences in mineralogy between the LF shales in Areas 1 and 2, which may be related to the differences in the transverse distribution of the LF shales in the Sichuan Basin.

Meanwhile, Chen et al. (2011b) indicated that the clay minerals contents of the LF shales from the Changning-Wenxin region in the Sichuan Basin ranged from 16.8% to 70.1%, with an average of 53.4%, whereas the quartz contents were between 16.2% and 75.2%, with a mean value of 29.2%, and the carbonates contents ranged from 0% to 20.1% with an average of 6.98%. Chen et al. (2013b) found that the clay minerals contents of the LF shales from the Changxin well 1 in the Sichuan Basin ranged from 15% to 75%, with an average of 40%; the quartz contents ranged from 30% to 70%, with a mean value of 34%; and the carbonate contents ranged from 5% to 30%, with an average of 18%. For Jiaoye well 1 in the Jiaoshiba region of the Sichuan Basin, Guo et al. (2013) showed that the average clay minerals content of LF shales was 34.6%, the average quartz contents was 37.39%, and the average carbonates content was 9.71%. Our test data differ from the results of Chen et al. (2011b, 2013b) and Guo et al. (2013), possibly because of the heterogeneous distribution of the LF shales. However, our results agree with previous studies showing that the mineralogical compositions of the LF shales in the Sichuan Basin are dominated by quartz and clay minerals.

A comparison of the mineralogy of the ULF and LLF shale samples in Areas 1 and 2 is shown in Table 1. Table 1 demonstrates that there are greater mineralogical differences between the ULF shale samples and LLF shale samples within each area than between Areas 1 and 2. It is also clear from Table 1 that the quartz contents of the ULF shales are lower than these of the LLF shales. The average quartz content of the ULF shales is 27.6% and 29.02% in Area 1 and Area 2, respectively, whereas the average quartz content of the LLF shales is 52.19% and 41.10% in Area 1 and Area 2, respectively. The clay minerals contents are higher in ULF than in LLF shales. The average clay minerals content of the ULF shales is 47.09% and 58.70% in Area 1 and Area 2, respectively, and the average clay minerals content of the LLF shales is 14.52% and 27.71% in Area 1 and Area 2, respectively. Similarly, the carbonates content of the ULF shales is higher than that of the LLF shale. The average carbonates content of the ULF shales is 18.57% and 2.72% in Area 1 and Area 2, respectively, and the average carbonate content of the LLF shales is 29.86% and 13.74% in Area 1 and Area 2, respectively. These mineralogical differences between the ULF shales and the LLF shales lead to differences in term of physiochemical and brittleness characteristics, which have implications for wellbore stability during the drilling as well as the fracture network during the hydraulic fracturing of shale formations.

3.2. TOC

The TOC contents of the LF shale samples for Area 1 and Area 2 are shown in Fig. 3 and Table 2. These results demonstrate that the TOC content of the ULF shale is lower than that of the LLF shale. For the ULF shale, the average TOC content in Area 1 is 1.25% (range: 1.06%–1.53%), whereas the average TOC content in Area 2 is 1.01% (range: 0.274%–3.26%). However, the average TOC content of LLF shale in Area 1 is 4.12% (range: 3.44–4.53%), and in Area 2 the average TOC content is 3.83% (range: 2.04%–5.87%). The results of Chen et al. (2013a,b) for Changxin well 1 showed an average TOC content for ULF shale of 1.40% (range: 1.04–2.05%) and an average

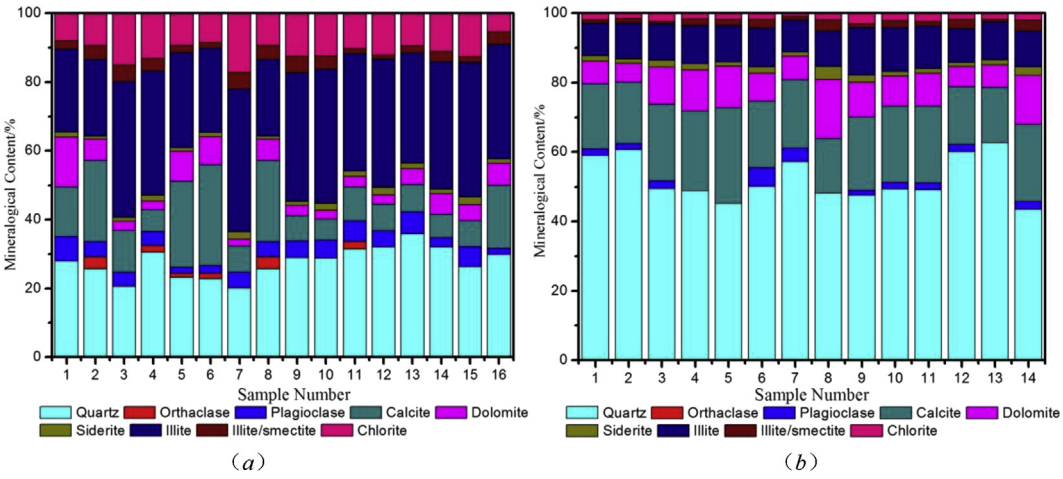

Fig. 1. XRD analysis results for ULF (a) and LLF (b) shale samples in Area 1.

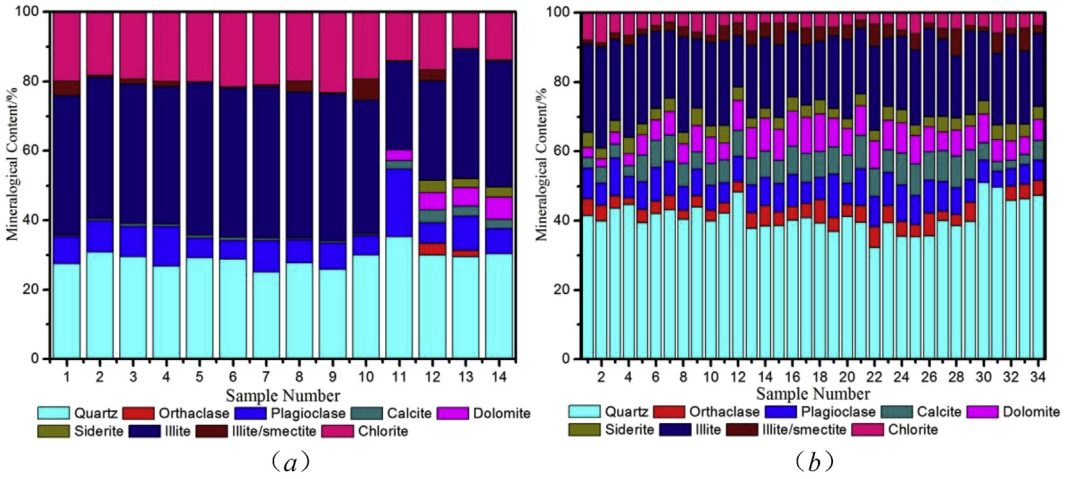

Fig. 2. XRD analysis results for ULF (a) and LLF (b) shale samples in Area 2.

Table 1
Comparison of the mineralogy of ULF and LLF shale samples in Areas 1 and 2.

Area	Formation	Quartz %			Clay minerals %			Carbonate %		
		Min	Max	Ave	Min	Max	Ave	Min	Max	Ave
Area 1	ULF	20.08	35.9	27.6	34.56	63.6	47.09	8.76	37.51	18.57
	LLF	43.46	62.66	52.19	11.1	18.79	14.52	22.4	39.59	29.86
Area 2	ULF	25.12	35.27	29.02	39.68	65.94	58.7	0.38	9.06	2.72
	LLF	32.25	51.04	43.10	21.45	39.08	25.71	5.97	18.63	13.74

Min = Minimum; Max = Maximum; Ave = Average; Clay minerals = illite + illite/smectite + chlorite; Carbonates = calcite + dolomite.

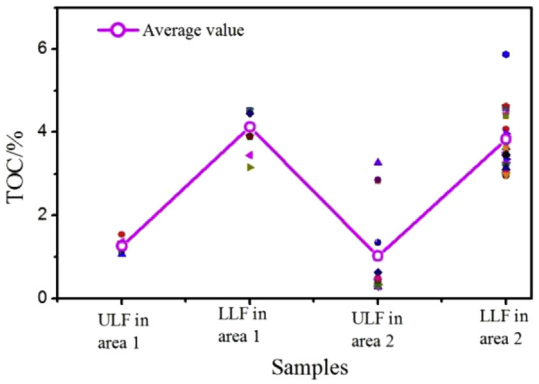

Fig. 3. TOC contents of the ULF and LLF shale samples in Areas 1 and 2.

TOC content for LLF shale of 5.33% (range: 3.95%–6.70%). These results align with our data showing that the LLF shales are richer in organic matter than the ULF shales.

The relationships between the quartz and TOC contents of the ULF and LLF shales are shown in Figs. 4 and 5, respectively. In Fig. 4, there is no apparent relationship between the quartz and TOC contents for the ULF shales in Area 1 (R^2 = 0.0793 in Fig. 4a), whereas there is a positive correlation between these variables for the LLF shales (R^2 = 0.538 in Fig. 4b). Similarly, in Fig. 5 we observe that there is no relationship between the quartz and TOC contents of the ULF shales in Area 2 (R^2 = 0.0481 in Fig. 5a), but that there is a positive relationship for the LLF shales (R^2 = 0.603 in Fig. 5b). As demonstrated by previous studies (Ross and Bustin, 2007; Chalmers et al., 2012), a positive relationship between quartz and TOC contents in shales indicates a biogenic origin of the quartz. Shales in those studies were from the Lower Jurassic (northeastern British Columbia, Canada) (Ross and Bustin, 2007) and Upper Devonian-Lower Mississippian (northeastern British Columbia, Canada) (Chalmers et al., 2012). Therefore, we propose that the ULF shale samples contain less quartz of biogenic origin, whereas the LLF shale samples contain more quartz of biogenic origin. Bai et al. (2013) suggested that the quartz in the ULF shales was primarily derived from terrigenous detrital material and that the quartz in the LLF shales was mainly derived from siliceous organisms. This finding may be observed because the LLF shales are deposited in deep water in a sedimentary environment with less terrigenous inputs from the coast. In contrast, the ULF shales were deposited in shallow water and probably received greater terrigenous inputs.

Table 2
Comparison of the TOC and CEC of the ULF and LLF shale samples in Areas 1 and 2.

Area	Formation	TOC %			CEC/mmol kg^{-1}		
		Min	Max	Ave	Min	Max	Ave
Area 1	ULF	1.06	1.53	1.25	70	120	94.69
	LLF	3.44	4.53	4.12	30	55	38.93
Area 2	ULF	0.274	3.26	1.01	–	–	–
	LLF	2.04	5.87	3.83	40	65	45.58

3.3. CEC

The CEC of shales is directly related to the water adsorption capacity and to surface hydration, which reflects the hydration expansion of shale. Therefore, CEC analysis was used to investigate the hydration expansion capacity of the shales. The CEC results for the LF shales are shown in Fig. 6 and Table 2. In Area 1, the CEC varies greatly between the ULF shales and the LLF shales. The CEC of the ULF shales ranges from 70 mmol/kg–120 mmol/kg, with an average of 94.69 mmol/kg. The CEC of the LLF shales ranges from

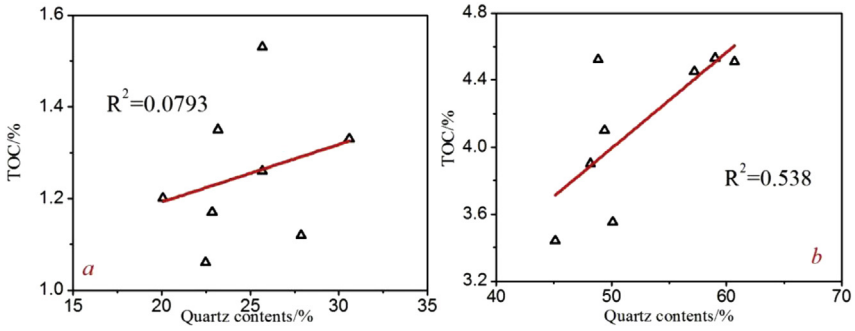

Fig. 4. Relationship between TOC and quartz contents of the ULF (a) and LLF (b) shale samples in Area 1.

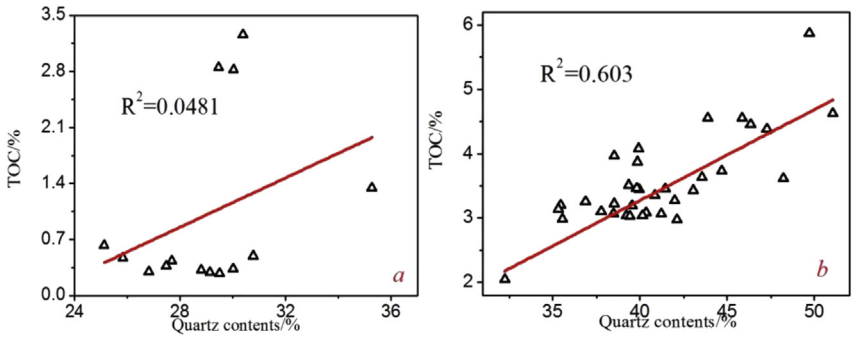

Fig. 5. Relationship between TOC and quartz contents of the ULF (a) and LLF (b) shale samples in Area 2.

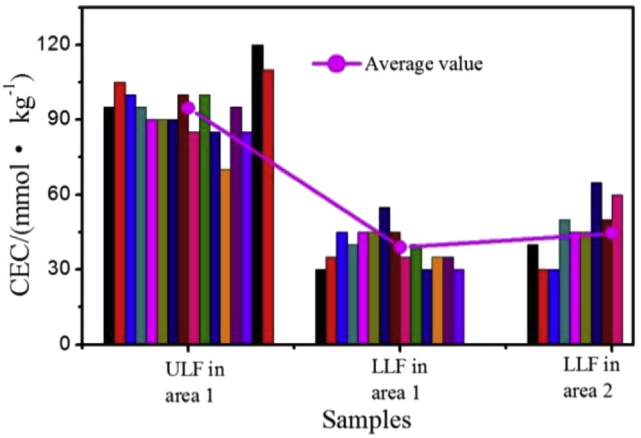

Fig. 6. CEC of the ULF and LLF shale samples in Areas 1 and 2.

30 mmol/kg to 55 mmol/kg, with an average of 38.93 mmol/kg. In Area 2, the average CEC of LLF shales is 45.58 mmol/kg, which is much lower than the CEC of the ULF shales in Area 1. These data show that CEC varies greatly between the ULF shales and the LLF shales. Additionally, the hydration expansion capacity of the ULF shales is greater than that of the LLF shales. The differences between the ULF shales and the LLF shales affect wellbore stability during drilling. To avoid potential collapse of a well, it will be important to prevent shale hydration during drilling in the ULF shale formation.

3.4. N_2 adsorption–desorption isotherms

The N_2 adsorption–desorption isotherms of some ULF and LLF shale samples in Area 1 are shown in Figs. 7 and 8, respectively. We observe that the N_2 adsorption–desorption isotherms of the ULF and LLF shales belong to the type IV category of isotherms (isotherms with a hysteresis loop), according to the BDDT (Brunauer, Deming, Deming and Teller) classification (Brunauer et al., 1940). This categorization suggests that the shale samples contain both mesopores and macropores (Sing et al., 1985). The N_2 adsorption–desorption isotherm at higher relative pressure showed a hysteresis loop because of capillary condensation (Gregg and Sing, 1992), indicating that the shale samples contain mesopores (Sing et al., 1985). Furthermore, from Figs. 7 and 8 we can observe that when the relative pressure is low, the adsorption branch of isotherms is coincident with the desorption branch. However, as the relative pressure increases, the adsorption branch and desorption branch gradually separate, which lead to form the hysteresis loop. The shape of the hysteresis loop indicates the morphology of pore shapes in solids (Sing et al., 1985). The desorption branches of the isotherms of the ULF and LLF shales do not show an inflection point. According to the International Union of Pure and Applied Chemistry (IUPAC) classification (Sing et al., 1985), the hysteresis loop shape of the N_2 adsorption–desorption isotherms of the ULF and LLF shales in Area 1 may be classified as type H3, which is usually associated with slit-shaped pores (Sing et al., 1985; Yang et al., 2014; Liu et al., 2015; Xiong et al., 2015).

Table 3 summarizes the results from the low-pressure N_2 adsorption/desorption analysis of the LF shale samples, including the specific surface area and total pore volume. The specific surface area of the ULF shale, calculated from N_2 adsorption data using the multipoint BET model, averages 8.133 m^2/g (ranges from 7.477 to 9.039 m^2/g) and the total pore volume of the ULF shale averages 0.01982 cm^3/g (varies from 0.01798 to 0.02072 cm^3/g); the specific surface area of the LLF shale averages 8.79 m^2/g (ranges from 8.100 to 9.331 m^2/g) and the total pore volume of the LLF shale exhibits a mean of 0.02206 cm^3/g (varies from 0.02105 to 0.02349 cm^3/g). The specific surface area and the total pore volume of the LLF shales are

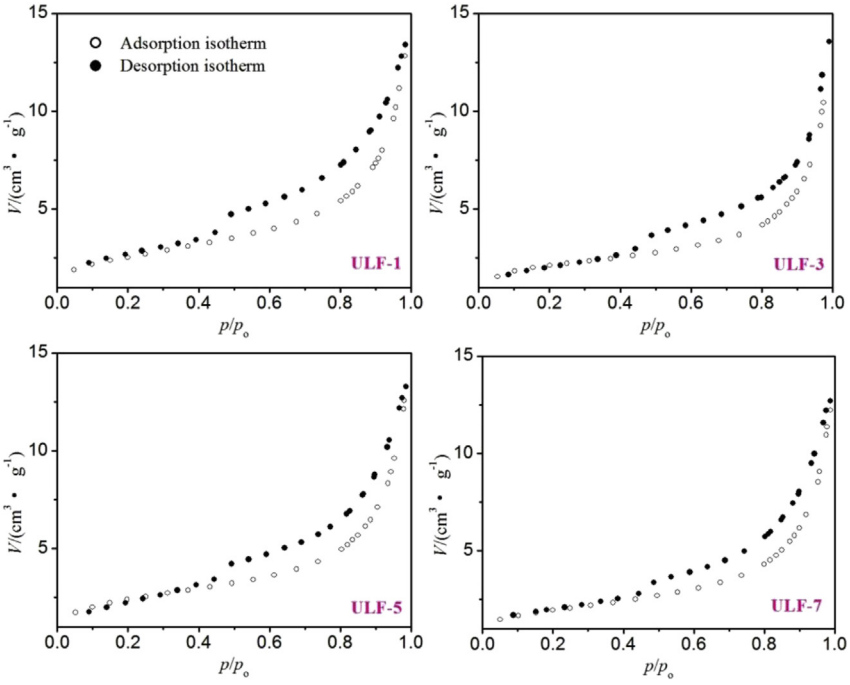

Fig. 7. The N_2 adsorption–desorption isotherms of some ULF shale samples in Area 1.

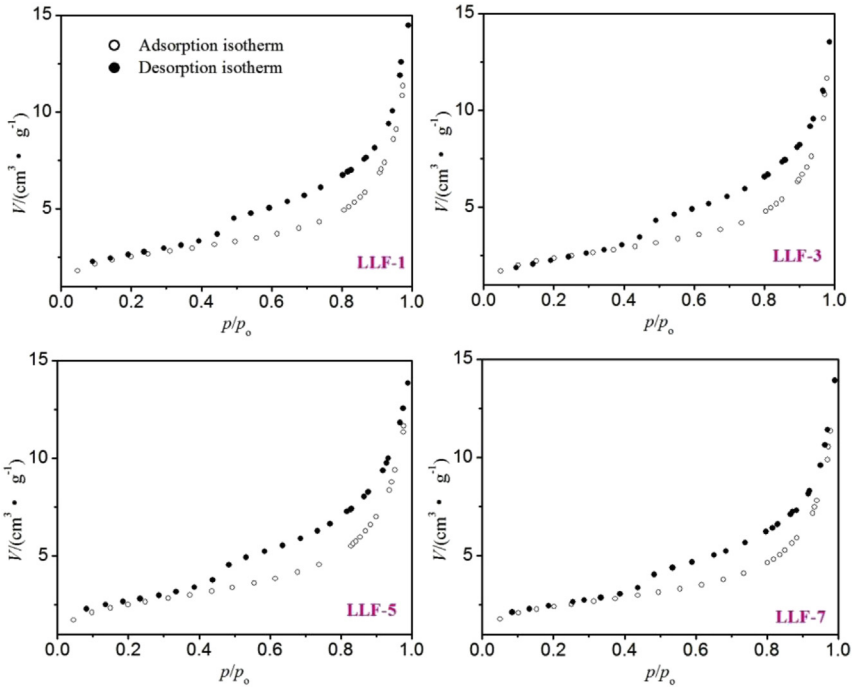

Fig. 8. The N_2 adsorption–desorption isotherms of some LLF shale samples in Area 1.

higher than those of the ULF shales, indicating that the LLF shales have better reservoir properties than the ULF shales. This finding is observed because the LLF shales have higher TOC content and contain a larger number of organic-matter pores (Yang et al., 2014), which results in higher specific surface area and total pore volume.

3.5. Fractal dimensions

The plots of $\ln(V)$ vs $\ln(\ln(p_0/p))$ of some ULF and LLF shale samples in Area 1 are presented in Figs. 9 and 10, respectively. We observe that there is a straight line segment through the whole relative pressure range, and we obtain a slope with piecewise fitting. The fractal dimension D is calculated from the linear segment, as shown in Table 3. We observe that all of the correlation coefficients are greater than 0.99, suggesting that there are fractal characteristics of the ULF and LLF shales. In addition, Table 3 indicates that the fractal dimension D of the ULF shales ranges from 2.6005 to 2.6219 with a mean value of 2.6219 and

Table 3
Specific surface area and total pore volume of the LF shale samples in Area 1.

Number	Area	Samples	Specific surface area (m^2/g)[a]	Total pore volume (cm^3/g)[b]	Fractal	R^2
1	Area 1	Upper Longmaxi Formation shales	9.039	0.02071	2.6056	0.9968
2			8.563	0.02072	2.6219	0.9957
3			7.477	0.01996	2.6008	0.9975
4			7.589	0.02034	2.6058	0.9924
5			8.631	0.01957	2.6143	0.9961
6			7.978	0.01798	2.6083	0.9984
7			7.560	0.01884	2.6005	0.9971
8			8.23	0.02047	2.6126	0.9955
1		Lower Longmaxi Formation shales	9.013	0.02296	2.6464	0.9958
2			9.279	0.02349	2.648	0.9955
3			8.417	0.02105	2.6362	0.0.9974
4			9.331	0.02219	2.6471	0.9981
5			9.061	0.02146	2.6357	0.9921
6			8.100	0.02119	2.6363	0.9970
7			8.481	0.02259	2.6474	0.9965
8			8.640	0.02157	2.6356	0.9929

[a] Specific surface area is calculated by the BET method.
[b] Total pore volume is estimated to be the liquid volume of nitrogen at a relative pressure of 0.98.

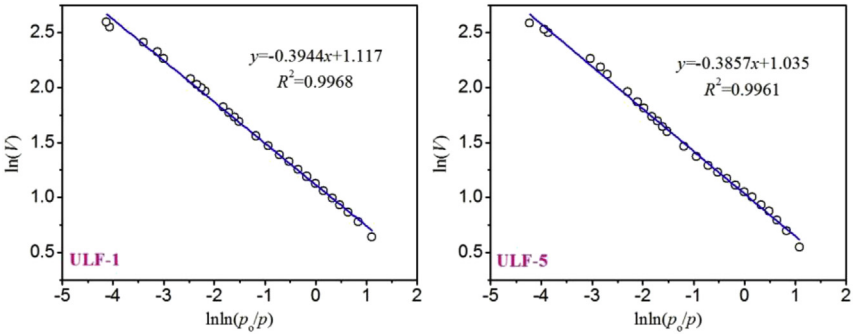

Fig. 9. Plots of ln(V) vs. ln(p_0/p)) reconstructed from the N_2 adsorption data of some of the ULF shale samples in Area 1.

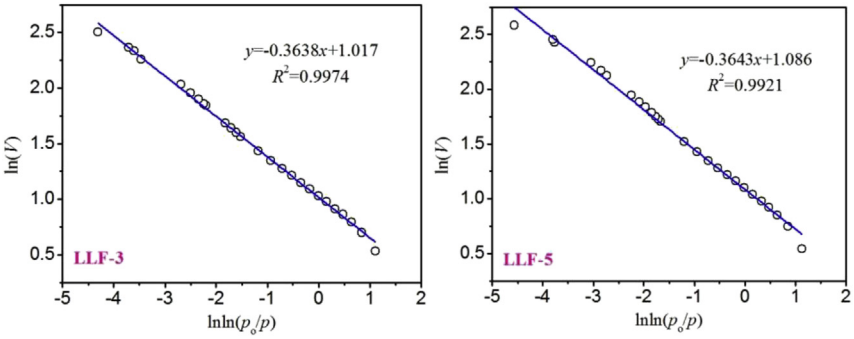

Fig. 10. Plots of ln(V) vs. ln(ln(p_0/p)) reconstructed from the N_2 adsorption data of some of the LLF shale samples in Area 1.

that the fractal dimension D of the LLF shales varies from 2.6365 to 2.6480 with an average of 2.6480. A greater fractal dimension D of the LLF shales compared to the ULF shales indicates that the LLF shales have greater roughness in terms of the pore surface and a more sophisticated pore structure than the ULF shales. This finding is observed because shales with a higher fractal dimension have a more irregular pore structure (Yang et al., 2014; Liu et al., 2015). This observation may be related to the fact that LLF shales with increased TOC contents have more micropores (Strąpoć et al., 2010; Loucks et al., 2012; Tian et al., 2013; Yang et al., 2014), leading to a more complex pore structure and consequently resulting in larger fractal dimensions. Yao et al. (2008) and Yang et al. (2014) confirmed that the adsorption capacity of coals or shales increased with the increase of fractal dimensions. However, Yao et al. (2009) and Cai et al. (2013) suggested that the pore structure in the coals had large effects on gas transport and that the coals with higher fractal dimensions had less flow capacity. Therefore, the adsorption capacity of the LLF shales may be higher and they may have a more complicated pore structure, which may inhibit gas desorption and lead to lower gas flow capability.

3.6. SEM imaging

The SEM images of the microstructures of the ULF and LLF shale samples in Area 1 are shown in Figs. 11 and 12, respectively. The

ULF and LLF shales have flaky clay minerals particles that are aligned in the direction of bedding. In a macroscopic view, the shales show well-developed bedding and micro-fractures (cracks) in the bedding interlay. In the ULF shales, clay minerals and non-clay minerals particles are distributed randomly and have weak particle bonding. The LLF shales have well-developed corrosion pores. In addition, Figs. 11c,d and 12c,d show that the matrix in the LF shales has well-developed micro-fractures. The LLF shales have a higher degree of fracture development than the ULF shales.

3.7. Wetting

The contact angles of the LF shale samples are shown in Fig. 13 and Table 4. It is obvious that the LF shale surface is both water-wet and oil-wet at the gas–liquid rock system, as indicated by the low contact angle. In other words, the shale wettability is mixed and inclined towards oil-wetting. Furthermore, the water contact angles vary among the shale samples, and these differences may be related to the TOC content (Liang et al., 2015). The oil and water wettability of the shale indicates the ability of water or oil to enter the shale by self-absorption under the influence of the capillary force. When water and oil enter into micro-fractures, the capillary force creates a wedge effect, causing wellbore instability. After water enters the shale and comes into contact with clay mineral, hydration and wedging effects occur at the crack tip, aggravating wellbore instability. Therefore, except for hydration inhibition, the oil-based drilling system has no advantage over a water-based drilling system in maintaining wellbore stability.

4. Discussions

4.1. Mineralogy characteristics

The XRD analysis results of the Longmaxi Formation shale samples from Area 1 and Area 2 demonstrate the presence of the same major inorganic minerals, including quartz, clay minerals, feldspar, carbonate, pyrite and siderite (Figs. 1 and 2). In Fig. 14, the quartz, carbonate and clay minerals contents are plotted in a ternary diagram showing that the LLF shale samples are richer in quartz, whereas the ULF shale samples are more clay-dominated.

The mineralogical compositions of the shales in this study were compared with well-known marine shales in the U.S. for which published data are available, including Barnett shale (Bowker, 2003; Bruner and Smosna, 2011), Woodford shale (Abousleiman et al., 2008), Marcellus shale (Bruner and Smosna, 2011) and New Albany shale (Strąpoć et al., 2010). The minimum and maximum values for typical minerals in shales are illustrated in Fig. 15. Compared with marine shales in the U.S., the LLF shales have higher quartz contents and the ULF shales have higher clay minerals contents. In contrast, the feldspar contents of the ULF and LLF shales in Area 1 (outcrop samples) are lower than in U.S. shales, and the feldspar contents of the ULF and LLF shales in Area 2 (core samples) are slightly higher than in some U.S. shales including the Barnett, Woodford and Marcellus shales. The carbonates contents of the LF shales in Area 2 (core samples) are lower than in U.S. shales, but the LF shales from Area 1 (outcrop samples) show higher carbonates contents than the Barnett, Woodford and New Albany shales. The LLF shales are similar to the Barnett shales in terms of quartz and clay minerals contents.

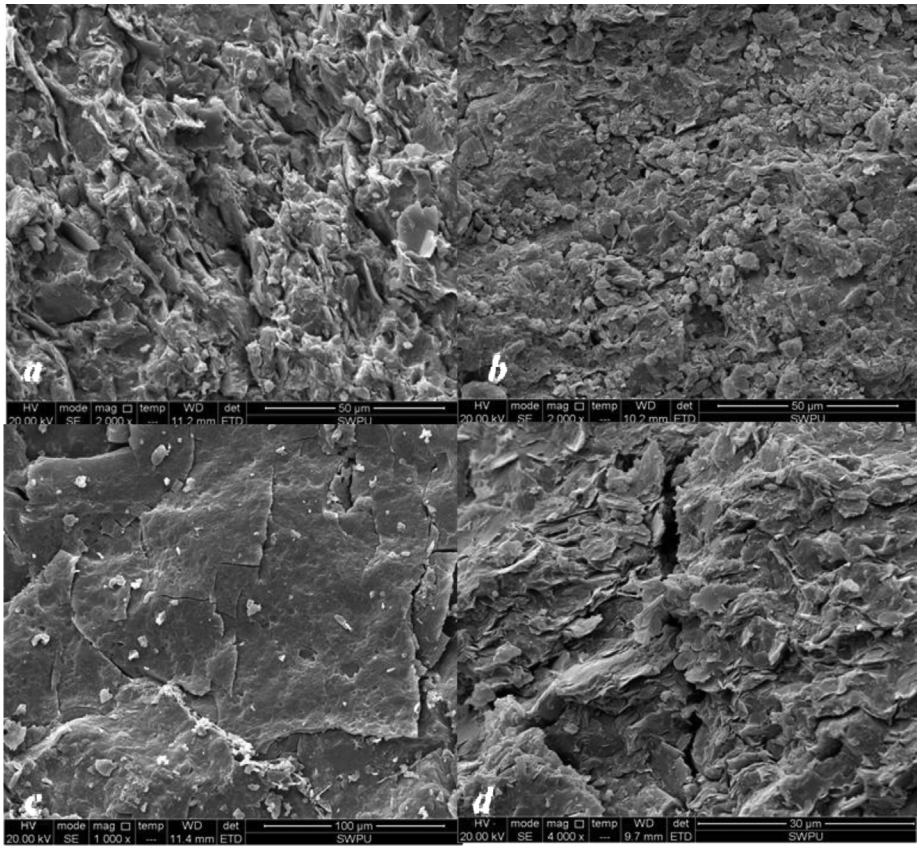

Fig. 11. SEM images of the ULF shale samples from Area 1: a) flaky clay minerals particles; b) clay minerals particles and non-clay minerals particles; c) and d) micro-fractures.

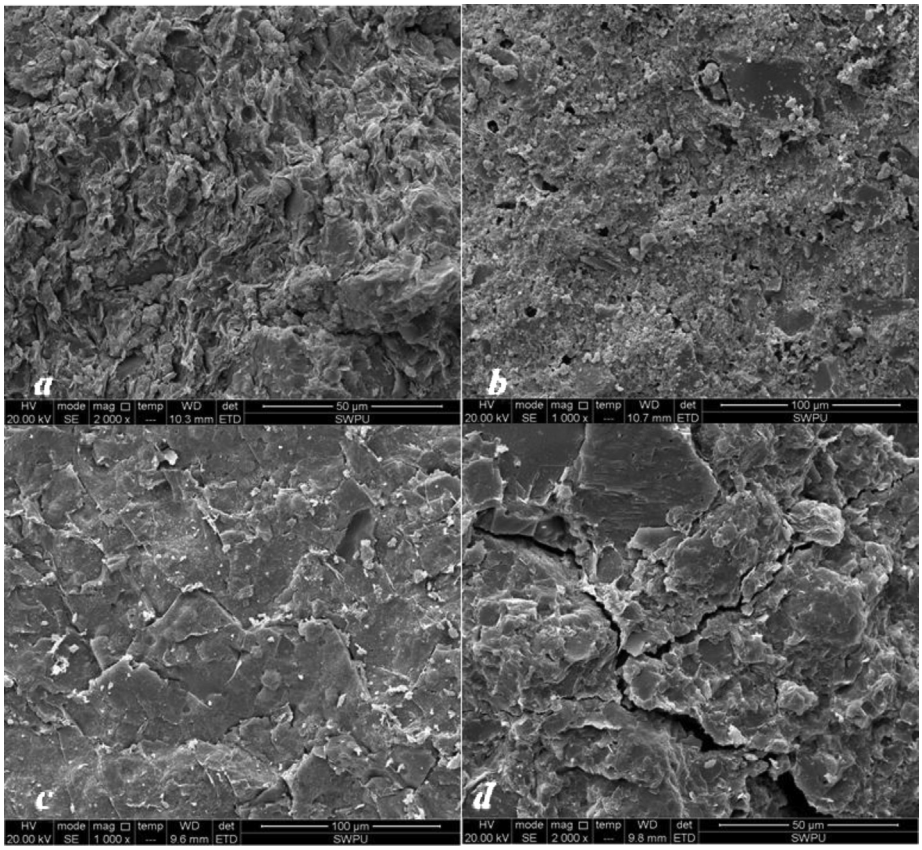

Fig. 12. SEM images of the LLF shale samples from Area 1: a) flaky clay minerals particles; b) corrosion pores; c) and d) micro-fractures.

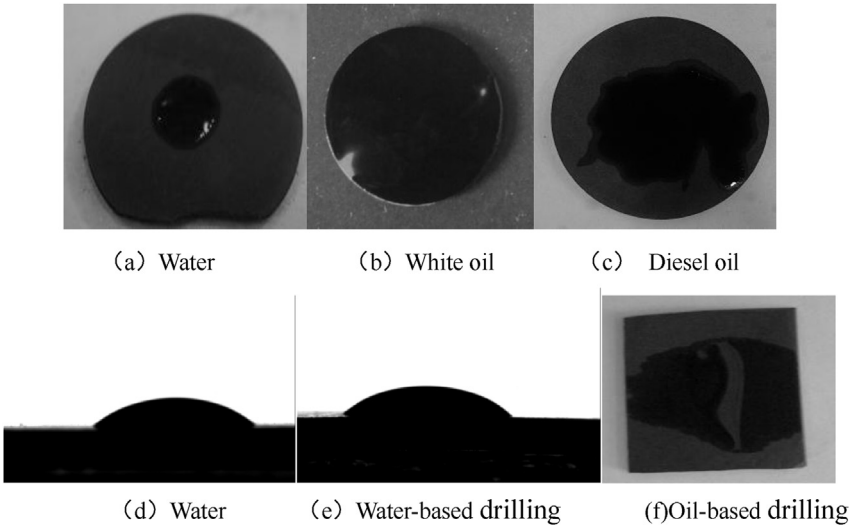

Fig. 13. Experimental contact angle results for the LF shale samples.

The brittleness of shale is the key to its stimulation, which is used to estimate the capacity to create a fracture network in a shale gas reservoir (Jarvie et al., 2007). High contents of brittle minerals make a reservoir highly brittle and make it easier to create network fractures and achieve volume reformation. The brittleness of shale is related to its mineralogy, and quartz has an important influence. The brittleness index of shale is given by Brittleness = Q/(Q + C + Cly) (Jarvie et al., 2007), where Q is the quartz contents, C is the calcite contents, and Cly is the clay minerals contents. The brittleness index of the LF shales is shown in Fig. 16, the LLF shales have a higher brittleness index than the ULF shales. In Area 1, the average brittleness index of the ULF shales is 31.43, whereas the average brittleness index of the LLF shales is 59.89. In Area 2, the average brittleness index of the ULF shales is 32.84, whereas the average brittleness index of the LLF shales is 53.03. There is no notable difference between the outcrop and core shale samples.

Table 4
Experimental contact angle results for the LF shale samples.

Liquid	ULF shales		LLF shales	
	CA[L]/°[a]	CA[R]/°[b]	CA[L]/°[a]	CA[R]/°[b]
Water-based drilling	33.9	33.9	40.4	40.4
	29.4	29.4	36.6	36.6
Oil-based drilling	Spreading	Spreading	Spreading	Spreading
Water	10.5	10.5	14.4	14.4
	11.6	11.6	17.7	17.7
White oil	Spreading	Spreading	Spreading	Spreading
Diesel oil	Spreading	Spreading	Spreading	Spreading

[a] The left contact angle.
[b] The right contact angle.

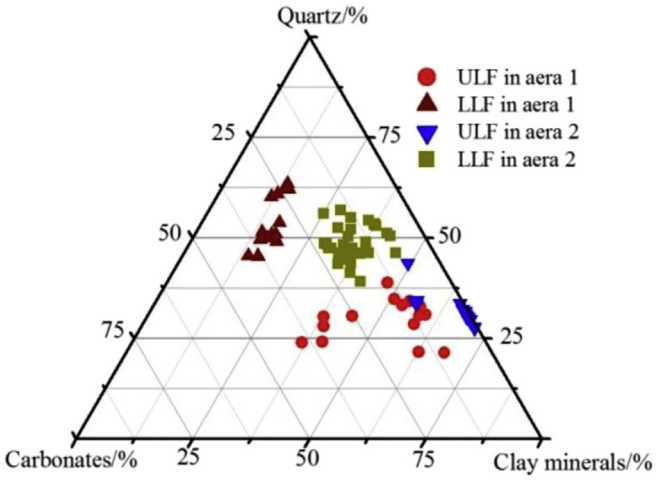

Fig. 14. Ternary diagram of the mineralogical compositions of the ULF and LLF shale samples from Areas 1 and 2.

The LLF shales are more brittle than the ULF shales in the Sichuan Basin, indicating that the LLF shale formation can more easily form network fractures, facilitating shale exploitation. According to Bowker (2002), the Barnett Shale showed an average quartz content of 45% and an average clay minerals content of 30%. The average compositions of the ULF shales are less than 30% quartz and more than 40% clay mineral. The average compositions of the LLF shales are more than 40% quartz and less than 30% clay mineral. The

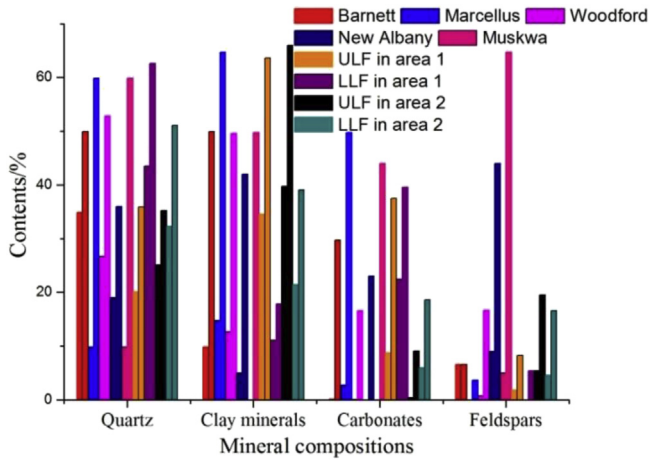

Fig. 15. Typical mineralogical compositions of the Barnett, Woodford, Marcellus, New Albany, ULF and LLF shales from Area 1 and 2.

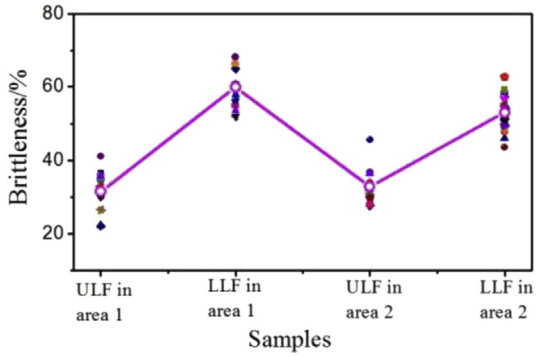

Fig. 16. Brittleness of the ULF and LLF shale samples in Area 1 and Area 2.

mineralogical compositions (quartz, calcite and clay mineral) of the shales from the Barnett, ULF and LLF shales are summarized in a ternary diagram (Fig. 17). We note that compared with the Barnett shale, the LLF shales have higher quartz contents, which imply a higher brittleness index. However, the ULF shales have higher clay minerals contents, which indicate a lower brittleness index. Therefore, the LLF shale formation is more brittle, which would allow the reservoir to form natural fractures and network fractures more easily. This results in accelerated desorption, diffusion and percolation of gas in shale and also accelerates the process of shale gas reservoir exploitation. Ding et al. (2012) analysed the relationship between the TOC contents and the degree of fracture development and suggested that the degree of fracture development increased with increasing TOC contents. We conclude that the degree of fracture development in the LLF shales is higher than in the ULF shales. The LLF shale formation has better physiochemical characteristics (lower CEC value) and greater brittleness, making hydraulic fracturing easier; thus, the LLF shales are more suitable for exploitation.

4.2. Relationships between mineralogy, TOC and specific surface area, total pore volume

The influences of mineralogical compositions and TOC on the specific surface area and total pore volume are displayed in Figs. 18 and 19. TOC is positively correlated with both specific surface area and total pore volume of the LF (ULF and LLF) shale samples (Figs. 18a and 19a, respectively). The relationships indicate that the LF shale samples with higher TOC contents have greater specific surface area and total pore volume, which is in agreement with previous studies (Chalmers et al., 2012; Tian et al., 2013; Liu et al., 2015; Xiong et al., 2015) indicating that organic matter strongly influences specific surface area and total pore volume.

The relationships of specific surface area and total pore volume to mineralogical composition of the LF shale samples are presented in Figs. 18 and 19, respectively. Quartz contents are positively related to both specific surface area and total pore volume (Figs. 18b and 19b, respectively), whereas clay mineral contents are negatively related to specific surface area and total pore volume (Figs. 18c and 19c, respectively). Higher total pore volume or specific surface area of shale is related to higher TOC contents, and the TOC contents increases with increasing quartz and decreasing clay minerals contents. These results agree with previous studies of marine shales (Chalmers et al., 2012) suggesting that the specific surface area and total pore volume increase with increasing quartz contents. However, studies on continental shales (Liu et al., 2015) have shown that the specific surface area and total pore volume

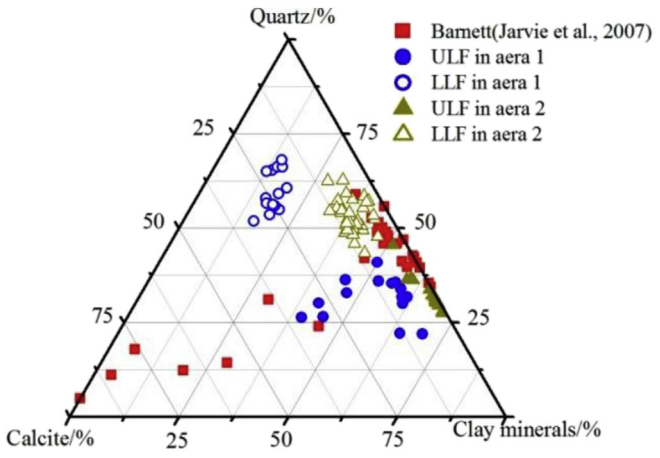

Fig. 17. Ternary diagram of the mineralogical compositions of the Barnett, ULF and LLF shales.

can improve the degree of contact between drilling fluid, clay minerals and organic matter, aggravating rock weaknesses and wellbore instability.

In terms of rock mechanics, any type of drilling fluid system that enters into a fracture will decrease the cohesion and angle of internal friction, which also weakens wellbore stability. Therefore, it is necessary to ensure that the drilling fluid has a good sealing ability and can control the loss of water, which would prevent the drilling fluid from entering micro-fractures. In organic-rich LF shales, if oil-based drilling fluid enters into the shale formation, it also weakens the rock (Liu et al., 2014; Liang et al., 2015). To avoid wellbore instability in the LF shale formation, it is important to choose a fluid with a strong sealing ability so that the drilling fluid system can form a seal in the wall, preventing drilling fluid from entering the formation. The appropriate bridging ion depends on the width of the fracture. For both oil- and water-based drilling fluid systems, the sealing technology of the fracture is an important consideration for the LF shale formation. For water-based drilling

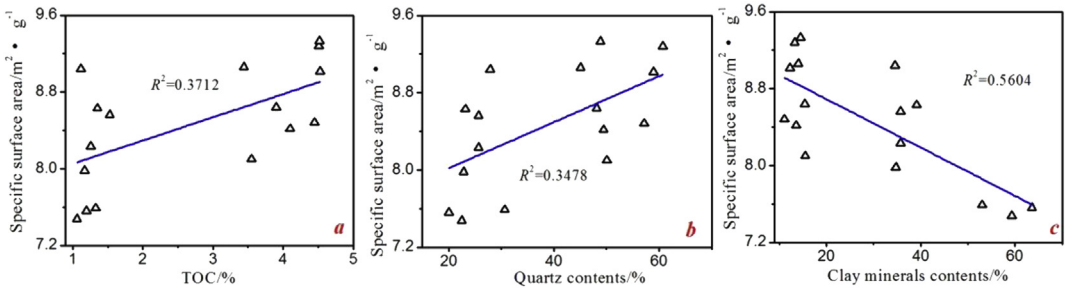

Fig. 18. Relationships between specific surface area and (a) TOC, (b) quartz contents and (c) clay minerals contents.

increase as quartz contents decrease. These differences could be related to different origins of the quartz in shales. Our results suggest that organic matter and quartz have a positive influence on the specific surface area and total pore volume for the LF shales, whereas the clay minerals have a negative influence.

4.3. The influence of microstructure

SEM characterization shows that the LF shales have clear bedding and various types of micro-fracturing (Figs. 11 and 12). Micro-fractures can destroy the integrity of shale, weakening the rock. However, micro-fractures can allow fluid movement through rock and also provide hydration space. Previous research (Liang et al., 2015) has shown that both oil and water can increase the stress at the tip of a crack, making it easier for cracks to expand and extend. Therefore, with positive differential pressure, drilling fluid can enter a formation through micro-fractures, triggering splitting action and destroying rock formations. In addition, micro-fractures

systems, it is necessary to consider hydration inhibition, especially for the ULF shale formation.

The micro-fractures in shale formations are the primary channels for free gas accumulation and thus a necessary route for shale gas transported to the bottom of well. Compared with the surrounding matrix, fractures have high permeability. When a shale gas reservoir begins production, the free gas in the fractures will come out first. The greater the number of fractures, the more free gas is available. More fractures will cause the pressure to decline in shale formations, allowing for shale gas desorption on the surface of mineralogical particles and organic matter. As weak surfaces, micro-fractures may concentrate stress during hydraulic fracturing, expanding at their tips and connecting with each other. Therefore, well-developed fractures can assist in hydraulic fracturing by forming complex network fracture systems. This process also helps free and desorbed gas to reach the bottom of the shale gas well, thereby improving shale gas production.

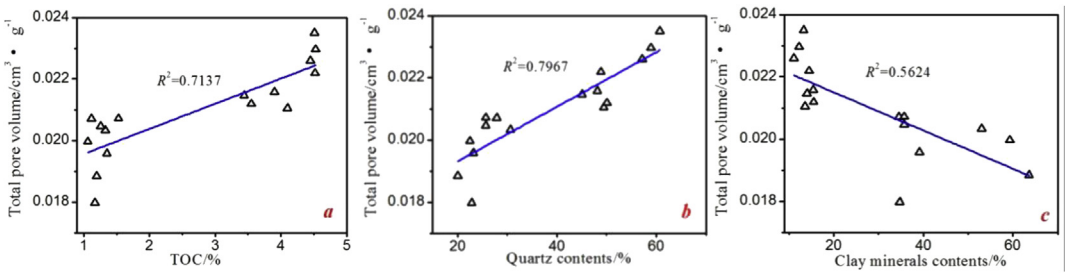

Fig. 19. Relationships between total pore volume and (a) TOC, (b) quartz contents and (c) clay minerals contents.

5. Conclusions

In this paper, the different properties of the LLF and ULF shales in the Sichuan Basin of China were investigated, including mineralogical characteristics, microstructural characteristics and physiochemical characteristics. The following conclusions can be made:

(1) The LF shales in the Sichuan Basin consist mainly of quartz and clay minerals. The ULF shales have higher clay minerals contents and lower quartz contents, whereas the LLF shales have lower clay minerals contents and higher quartz contents.
(2) Compared with the ULF shales, the LLF shales have higher TOC contents, which results in a higher specific surface area and total pore volume, a larger fractal dimension and a more complex pore structure, which in turn leads to a greater adsorption capacity.
(3) Compared with the ULF shales, the LLF shales have a weaker hydration swelling effect and more brittle features, indicating that the LLF shales would promote good wellbore stability and hydraulic fracturing.
(4) Because of fractures in the LF shale formation, the designs of oil-based or water-based drilling fluid systems need to consider sealing technologies. For water-based drilling systems, hydration inhibition should be considered, especially for the ULF shale formation.

Acknowledgments

This research was supported by the United Fund Project of National Natural Science Foundation of China (Grant No.U1262209) and the National Natural Science Foundation of China (NSFC) (Grant No.51274172).

References

Avnir, D., Jaroniec, M., 1989. An isotherm equation for adsorption on fractal surfaces of heterogeneous porous materials. Langmuir 5, 1412–1433.
Abousleiman, Y.N., Tran, M.H., Hoang, S.K., Ulm, F.J., Bobko, C.P., Ortega, J.A., 2008. Study characterizes Woodford shale. Am. Oil Gas Report. 51 (1), 106–115.
Brunauer, S., Emmett, P.H., Teller, E., 1938. Adsorption of gases in multimolecular layers. J. Am. Chem. Soc. 60, 309–319.
Brunauer, S., Deming, L.S., Deming, W.E., Teller, E., 1940. On a theory of the van der Waals adsorption of gases. J. Am. Chem. Soc. 62 (7), 1723–1732.
Bowker, K.A., 2003. Recent development of the Barnett Shale play. Ft. Worth Basin West Tex. Geol. Soc. Bull. 42 (6), 1–11.
Bruner, K., Smosna, R., 2011. A Comparative Study of the Mississippian Barnett Shale, Fort Worth Basin, and Devonian Marcellus Shale. National Energy Technology Laboratory (NETL) for The United States Department of Energy. Technical Report, Appalachian Basin: Technical Report DOE/NETL-2011/1478.
Bai, Z., Liu, G., Sun, W., Ran, B., Luo, C., Yang, D., Wang, S., Zhang, X., 2013. Reservoir characteristic of Wufeng Formation – Longmaxi Formation in southwest of Sichuan Basin, China. J. Chengdu Univ. Technol. Technol. Ed. 40 (5), 521–531.
Chen, S., Zhu, Y., Wang, H., Liu, H., Wei, W., Fang, J., 2011a. Shale gas reservoir characterization: a typical case in the southern Sichuan Basin of China. Energy 36, 6609–6616.
Chen, S., Zhu, Y., Wang, H., Liu, H., Wei, W., Fang, J., 2011b. Characteristics and significance of mineral compositions of Lower Silurian Longmaxi Formation shale gas reservoir in the southern margin of Sichuan Basin. Acta Pet. Sin. 32 (5), 775–782.
Chen, S., Zhu, Y., Wang, H., Liu, H., Wei, W., Fang, J., 2012. Structure characteristics and accumulation significance of nanopores in Longmaxi shale gas reservoir in the southern Sichuan Basin. J. China Coal Soc. 37 (3), 438–444.
Chalmers, G.R.L., Ross, D.J.K., Bustin, R.M., 2012. Geological controls on matrix permeability of Devonian Gas Shales in the Horn River and Liard basins, northeastern British Columbia, Canada. Int. J. Coal Geol. 103, 120–131.
Chen, S., Xia, X., Qin, Y., Fu, C., Hu, L., 2013a. Classification of pore structures in shale gas reservoir at the Longmaxi Formation in the south of Sichuan Basin. J. China Coal Soc. 37 (5), 760–765.
Chen, W., Zhou, W., Luo, P., Deng, H., Li, Q., Shan, R., Qi, M., 2013b. Analysis of the shale gas reservoir in the lower silurian longmaxi formation, changxin 1 well, southeast sichuan Basin, China. J. Acta Petrologica Sinica 29 (3), 1073–1086.
Cai, Y., Liu, D., Pan, Z., Yao, Y., Li, J., Qiu, Y., 2013. Pore structure and its impact on CH_4 adsorption capacity and flow capability of bituminous and subbituminous coals from Northeast China. Fuel 103, 258–268.
Cheng, W., Jin, Y., Chen, M., 2015. Reactivation mechanism of natural fractures by hydraulic fracturing in naturally fractured shale reservoirs. J. Nat. Gas Sci. Eng. 23, 431–439.
Ding, W., Li, C., Li, C., 2012. Fracture development in shale and its relationship to gas accumulation. Geosci. Front. 3 (1), 97–105.
Dai, J., Zou, C., Liao, S., Dong, D., Ni, Y., Huang, J., Hu, G., 2014. Geochemistry of the extremely high thermal maturity Longmaxi shale gas, southern Sichuan Basin. Org. Geochem. 74, 3–12.
Gregg, S.J., Sing, K.S.W., 1992. Adsorption, Surface Area, and Porosity. Academic Press.
Guo, W., Xiong, W., Gao, S., Hu, Z., Liu, H., Yu, R., 2013. Impact of temperature on the isothermal adsorption/desorption characteristics of shale gas. Petroleum Explor. Dev. 40 (4), 481–485.
Guo, T., Zhang, H., 2014. Formation and enrichment mode of Jiaoshiba shale gas field, Sichuan Basin. Petroleum Explor. Dev. 41 (1), 31–40.
Huang, W., Liu, S., Ma, W., Wang, G., Zeng, X., Wang, J., 2011. Shale gas exploration prospect of Lower Paleozoic in southeastern Sichuan and western Hubei-eastern Chongqing areas, China. Geol. Bull. China 30 (2/3), 364–371.
Huang, J., Zou, C., Li, J., Dong, D., Wang, S., Wang, S., Wang, Y., Li, D., 2012. Shale gas accumulation conditions and favorable zones of Silurian Longmaxi Formation in south Sichuan Basin,China. J. China coal Soc. 37 (5), 782–787.
Hou, Y., He, S., Yi, J., Zhang, B., Chen, X., Wang, Y., Zhang, J., Cheng, C., 2014. Effect of pore structure on methane sorption potential of shales. Petroleum Explor. Dev. 41 (2), 272–281.
Heng, S., Guo, Y., Yang, C., Daemen, J.J., Li, Z., 2015. Experimental and theoretical study of the anisotropic properties of shale. Int. J. Rock Mech. Min. Sci. 74, 58–68.
Jarvie, D.M., Hill, R.J., Ruble, T.E., Pollastro, R.M., 2007. Unconventional shale-gas systems: the Mississippian Barnett Shale of north-central Texas as one model for thermogenic shale-gas assessment. AAPG Bull. 91 (4), 475–499.
Liang, C., Jiang, Z., Yang, Y., Wei, X., 2012. Characteristics of shale lithofacies and reservoir space of the Wufenge-Longmaxi Formation, Sichuan Basin. Petroleum Explor. Dev. 39 (6), 691–698.
Loucks, R.G., Reed, R.M., Ruppel, S.C., Hammes, U., 2012. Spectrum of pore types and networks in mudrocks and a descriptive classification for matrix-related mudrock pores. AAPG Bull. 96 (6), 1071–1098.
Liu, S., Ma, W., Jansa, L., Huang, W., Zeng, X., Zhang, C., 2013. Characteristics of the shale gas reservoir rocks in the Lower Silurian Longmaxi Formation, East Sichuan Basin. Energy. Explor. Exploitation 31 (2), 187–220.
Liang, C., Chen, M., Jin, Y., Lu, Y., 2014. Wellbore stability model for shale gas reservoir considering the coupling of multi-weakness planes and porous flow. J. Nat. Gas Sci. Eng. 21, 364–378.
Liu, X., Xiong, J., Liang, L., Luo, C., Zhang, A., 2014. Analysis the wettability of Longmaxi Formation shale in the south region of Sichuan Basin and its influence. Nat. Gas. Geosci. 25 (10), 1644–1652.
Liu, X., Xiong, J., Liang, L., 2015. Investigation of pore structure and fractal characteristics of organic-rich Yanchang Formation shale in central China by nitrogen adsorption/desorption analysis. J. Nat. Gas Sci. Eng. 22, 62–72.
Liang, L., Xiong, J., Liu, X., 2015. Experimental study on crack propagation in shale formations considering hydration and wettability. J. Nat. Gas Sci. Eng. 23, 492–499.
Ministry of Land and Resources of the People's Republic of China (MLR), 2012. The Nation Survey and Evaluation of Shale Gas Resource and Favorable Area Selection. http://www.mlr.gov.cn/wszb/2012/yyqzy/.
Pfeifer, P., Avnir, D., 1983. Chemistry in noninteger dimensions between two and three. J. Chem. Phys. 79 (7), 3369–3558.
Ross, D.J.K., Bustin, R.M., 2007. Shale gas potential of the lower jurassic gordondale member, northeastern British Columbia, Canada. Bull. Can. Petroleum Geol. 55 (1), 51–75.
Sing, K.S.W., Everett, D.H., Haul, R.A.W., Moscou, L., Pierotti, R.A., Rouquerol, J., Siemieniewska, T., 1985. Reporting physisorption data for gas/solid systems with special reference to the determination of surface area and porosity. Pure Appl. Chem. 57 (4), 603–619.
Strąpoć, D., Mastalerz, M., Schimmelmann, A., Drobniak, A., Hasenmueller, N.R., 2010. Geochemical constraints on the origin and volume of gas in the New Albany Shale (DevonianeMississippian), eastern Illinois Basin. AAPG Bull. 94 (11), 1713–1740.
Tian, H., Pan, L., Xiao, X., Wilkins, R.W.T., Meng, Z., Huang, Z., 2013. A preliminary study on the pore characterization of Lower Silurian black shales in the Chuandong Thrust Fold Belt, southwestern China using low pressure N_2 adsorption and FE-SEM methods. Mar. Petroleum Geol. 48, 8–19.
Tang, X., Jiang, Z., Li, Z., Gao, Z., Bai, Y., Zhao, S., Feng, J., 2015. The effect of the variation in material composition on the heterogeneous pore structure of high-maturity shale of the Silurian Longmaxi Formation in the southeastern Sichuan Basin, China. J. Nat. Gas Sci. Eng. 23, 464–473.
U.S. Energy Information Administration (EIA), 2013. Technically Recoverable Shale Oil and Shale Gas Resources: an Assessment of 137 Shale Formations in 41 Countries outside the United States. http://www.eia.gov/analysis/studies/worldshalegas.
Wang, L., Zou, C., Zheng, P., Chen, S., Zhang, Y., Xu, B., Li, W., 2009. Geochemical evidence of shale gas existed in the Lower Paleozoic Sichuan Basin. Nat. Gas. Ind. 29 (5), 59–62.
Wang, Y., Dong, D., Li, J., Wang, S., Li, X., Wang, L., Cheng, K., Huang, J., 2012. Reservoir characteristics of shale gas in Longmaxi Formation of the Lower

Silurian, southern Sichuan. Acta Pet. Sin. 33 (4), 551–561.
Wu, J., Yu, B., Li, Y., 2012. Adsorption capacity of shale gas and controlling factors from the Well Yuye 1 at the southeast of Chongqing. J. Southwest Petroleum Univ. Technol. Ed. 34 (4), 40–48.
Wang, Y., Dong, D., Yang, H., He, L., Wang, S., Huang, J., Pu, B., Wang, S., 2014. Quantitative characterization of reservoir space in the Lower Silurian Longmaxi Shale, southern Sichuan, China. Sci. China Earth Sci. 57 (2), 313–322.
Xue, H., Wang, H., Liu, H., Yan, G., Guo, W., Li, X., 2013. Adsorption capacity and aperture distribution characteristics of shales: taking the Longmaxi Formation shale of Sichuan Basin as an example. Acta Pet. Sin. 34 (5), 826–832.
Xiong, J., Liu, X., Liang, L., 2015. Experimental study on the pore structure characteristics of the Upper Ordovician Wufeng Formation shale in the southwest portion of the Sichuan Basin, China. J. Nat. Gas Sci. Eng. 22, 530–539.
Yao, Y., Liu, D., Tang, D., Tang, S., Huang, W., 2008. Fractal characterization of adsorption-pores of coals from North China: an investigation on CH_4 adsorption capacity of coals. Int. J. Coal Geol. 73, 27–42.
Yao, Y., Liu, D., Tang, D., Tang, S., Huang, W., Liu, Z., Che, Y., 2009. Fractal characterization of seepage-pores of coals from China: an investigation on permeability of coals. Comput. Geosciences 35 (6), 1159–1166.
Yang, F., Ning, Z., Liu, H., 2014. Fractal characteristics of shales from a shale gas reservoir in the Sichuan Basin, China. Fuel 115, 378–384.
Zeng, X., Liu, S., Huang, W., Zhang, C., 2011. Comparison of Silurian Longmaxi Formation shale of Sichuan Basin in China and Carboniferous Barnett Formation shale of Fort Worth Basin in United States. Geol. Bull. China 30 (2/3), 372–384.
Zhang, Z., Hu, P., Shen, J., Rao, W., Li, W., 2013. Mineral compositions and organic matter occurrence modes of Lower Silurian Longmaxi Formation of Sichuan Basin. J. China coal Soc. 38 (5), 766–771.
Zhou, Q., Xiao, X., Tian, H., Pan, L., 2014. Modeling free gas content of the Lower Paleozoic shales in the Weiyuan area of the Sichuan Basin, China. Mar. Petroleum Geol. 56, 87–96.